JOURNAL OF MAGNETIC RESONANCE, Series A 102, 29–33 (1993)

Effects of Double Rotation on Homonuclear Spin Systems

Y. WU,* Z-Y. PENG, Z. OLEJNICZAK, B. Q. SUN, AND A. PINES

Lawrence Berkeley Laboratory and University of California, Berkeley, California 94720

Received February 13, 1992; revised June 26, 1992

The behavior of a homonuclear dipole-coupled spin system under double rotation (DOR) is investigated by nuclear magnetic resonance. We demonstrate, for a highly degenerate many-body spin system, that the coherence created by the fast spinning motion in DOR is not destroyed by the slow precession motion even when the precession frequency is significantly smaller than the dipole–dipole interactions. Therefore, the DOR technique can also be used to reduce line broadening arising from dipole–dipole interactions. © 1993 Academic Press, Inc.

INTRODUCTION

Spin Hamiltonians in NMR can be rendered time dependent by mechanical sample motions such as magic-angle spinning (MAS) and double rotation (DOR). Under MAS, originally introduced in the 1950s as a means to reduce homonuclear dipole–dipole couplings $\mathscr{H}_D$ (*1*), the sample is spun rapidly about a fixed axis inclined at the magic angle ($\beta_p = 54.74°$) with respect to the external magnetic field. Double rotation, developed recently as a coherent averaging technique for second-order quadrupolar interactions, imposes a more complex motion in which the axis of the sample rotor undergoes an additional slow precession about a second axis inclined at β_p. The trajectory is illustrated in Fig. 1 and is realized with a double rotor in which the angle between the axes of the inner and outer rotors is β_s (*2*). The sample is placed in the small inner rotor, which rotates with an angular velocity ω_s, while the larger outer rotor rotates at the magic angle with angular velocity ω_p.

Intuitively one might expect that any dipolar line narrowing achieved by rapid rotation of the small rotor ($\omega_s > \|\mathscr{H}_D\|$) would be destroyed by the slow precession of the inner rotor axis if the secondary precession frequency, ω_p, is smaller than $\|\mathscr{H}_D\|$. In this work, however, we demonstrate that an experimentally controllable phase γ can be created which is able to reverse the phases of the odd-numbered harmonics of the NMR signals. Similar behavior has been demonstrated for inhomogeneous interactions, such as quadrupolar interactions (*3*). This phenomenon offers proof that coherence created by the fast modulation is not destroyed by the slow modulation, even when ω_p is significantly smaller than $\|\mathscr{H}_D\|$. In this regard the effect is reminiscent of magic echoes in strongly coupled dipolar systems, which, through the phenomena of time reversal, provide a similarly vivid demonstration of coherent evolution (*4*).

EXPERIMENTAL

NMR signals of ^{23}Na were detected in a polycrystalline NaCl sample under DOR using a 400 MHz (proton) pulsed spectrometer. The DOR probe is described in detail elsewhere (*5*).

The relevant spin interactions in this system are the ^{23}Na Zeeman and homonuclear dipole–dipole interactions. The magnitude of $\mathscr{H}_D$ is approximately 2 kHz. Quadrupolar interactions vanish because the environment at each lattice site in NaCl is cubically symmetric, and inhomogeneous interactions between ^{23}Na and ^{35}Cl or ^{35}Cl are also not important for this study. The homogeneous character of the line broadening is consistent with the facts that linewidth cannot be reduced by the Hahn echo technique and is inversely proportional to the spinning speed under MAS.

THEORY AND RESULTS

Figure 2 compares a static spectrum of ^{23}Na in NaCl with DOR spectra obtained for two values of ω_p. In neither case were the RF pulses synchronized with the mechanical motions of the sample. At very slow precession, for example, 190 Hz, the spectrum in Fig. 2b, shows a pronounced centerband and several weaker sidebands separated by $\omega_s/2\pi = 2.6$ kHz. These latter signals are due to the harmonics of the spinning motion. When the spinning frequency is kept at 2.6 kHz but the precession frequency is increased to 323 Hz, the relatively broadbands collapse into sharp peaks of width 135 Hz as shown in Fig. 2c. The peaks are separated by $\omega_p/2\pi$, which corresponds to the harmonics of the precession motion. Interestingly, this effect occurs at a precession frequency much smaller than $\|\mathscr{H}_D\|$.

In the rotating frame, the dipole–dipole Hamiltonian truncated by the strong Zeeman interactions (*6*) is given, under DOR modulations, by

$$\mathscr{H}_D(t) = \sum_{nn'} e^{-in'\omega_p t} d^{(2)}_{n'0}(\beta_p) e^{-in\omega_s t} d^{(2)}_{nn'}(\beta_s) e^{-in'\gamma} S_n, \quad [1]$$

* Present address: Department of Physics and Astronomy, University of North Carolina, Chapel Hill, North Carolina 27599-3255.

1064-1858/93 $5.00

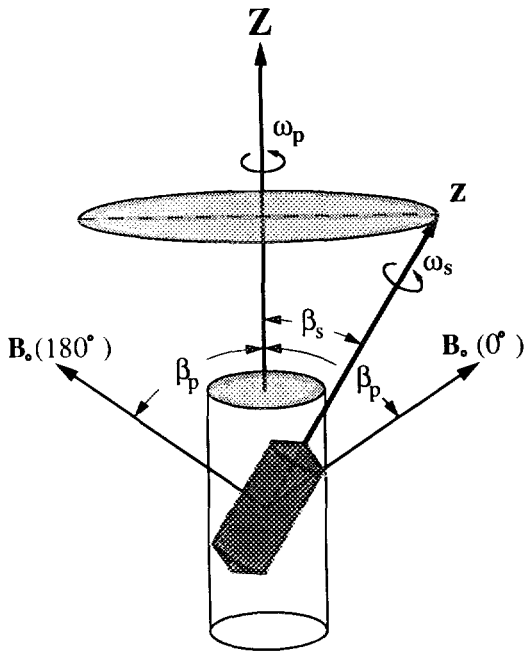

FIG. 1. The sample-containing inner rotor spins around the z axis at angular frequency ω_s while the z axis precesses around the Z axis at the angular frequency ω_p. The precession is imposed by the spinning motion of the outer rotor. The angle β_s is 30.56°, and the angle β_p between the external magnetic field B_0 and the Z axis is 54.74°. The relative orientations of B_0 at $\gamma = 0°$ and $\gamma = 180°$ are indicated by $B_0(\gamma = 0°)$ and $B_0(\gamma = 180°)$ with B_0 taken in the same plane as the z and Z axes.

in which

$$S_n = \sum_{i,j} D^{(2)}_{0n}(\Omega^{ij})\rho^{ij}_{20}T^{ij}_{20}. \qquad [2]$$

T^{ij}_{20} is the spherical tensor spin operator, while $D^{(2)}_{kl}$ and $d^{(2)}_{kl}$ represent the second-rank Wigner rotation matrix and the corresponding reduced matrix, respectively. The spatial spherical tensor of the dipole–dipole interactions for a spin pair (i, j) in the principal-axis system (PAS) is ρ^{ij}_{20}. The two sets of Euler angles, $\Omega_s = (\omega_s t, \beta_s, \gamma)$ and $\Omega_p = (\omega_p t, \beta_p, 0)$, describe the rotational transformations from the small rotor frame to the large rotor frame and from the large rotor frame to the laboratory frame, respectively. The angle γ depends on the orientation of the magnetic field relative to the axes of the two rotors at time $t = 0$, where time evolution starts. Two positions, $\gamma = 0°$ and $\gamma = 180°$, are illustrated in Fig. 1. The angle γ can be selected by synchronizing the RF pulses and the outer rotor. Effects of synchronization under MAS have also been investigated before (*7–9*). The Euler angles Ω^{ij}, which describe the rotational transformations from the PAS frame to the small rotor frame, depend on each particular spin pair (i, j). This system is clearly homogeneous (*7*) because operators T^{ij}_{20} and T^{jk}_{20} with a common index do not commute.

Assume now that the conditions $\omega_s > \|\mathscr{H}_D\|$ and $\omega_s \gg \omega_p$ are met. Then, according to the averaging method developed by Bogolyubov and Mitropol'skii (*10*), a solution of the density operator $\rho(t)$ can be sought in the form

$$\rho = \xi(t) + \sum_{k\neq 0} \rho_k(t)\exp(-ik\omega_s t), \qquad [3]$$

where $\xi(t)$ contains the time evolutions that are much slower than ω_s. This term describes the behavior of the centerband which arises from the spinning motion, where the corresponding sidebands are described by the harmonic terms $\rho_k(t)\exp(-ik\omega_s t)$. We should mention here that the effects of precessional motion are completely included in $\xi(t)$ and $\rho_k(t)$.

To apply the averaging method, we rewrite $\mathscr{H}_D(t)$ in Eq. [1] in the form

$$\mathscr{H}_D(t) = \sum_{n=-2}^{2} \mathscr{H}_n e^{-in\omega_s t}, \qquad [4]$$

with

$$\mathscr{H}_n = \sum_{n'} e^{-in'\omega_p t} d^{(2)}_{n'0}(\beta_p) d^{(2)}_{nn'}(\beta_s) e^{-in'\gamma} S_n. \qquad [5]$$

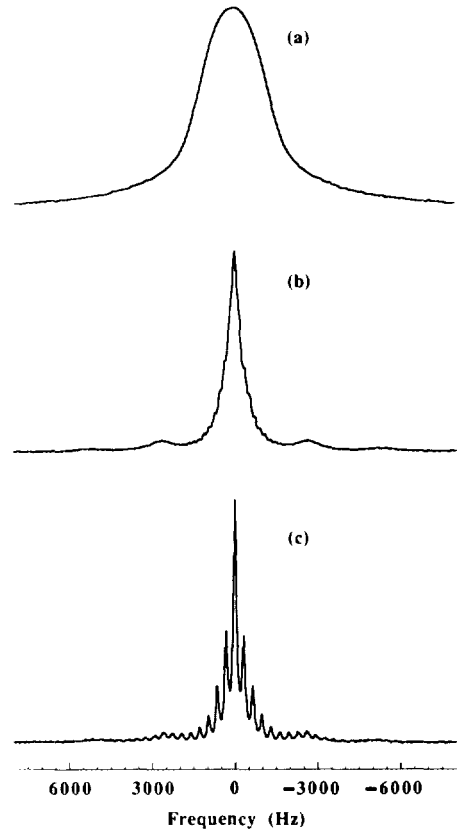

FIG. 2. (a) Static ^{23}Na spectrum of NaCl. (b) DOR spectrum with $\omega_s/2\pi = 2.6$ kHz and $\omega_p/2\pi = 190$ Hz; the broad sidebands associated with the spinning motion are clearly visible. (c) DOR spectrum with $\omega_s/2\pi = 2.6$ kHz and $\omega_p/2\pi = 323$ Hz; the broad frequency bands in (b) are split into various sharp peaks separated by $\omega_p/2\pi$.

The time evolution of $\xi(t)$ is, according to the averaging method, determined by $d\xi/dt = -i[\bar{\mathscr{H}}, \xi]$, where $\bar{\mathscr{H}}$ is the secular term of the Hamiltonian $\mathscr{H}_D$ with respect to the spinning motion. Up to order $\|\mathscr{H}_D\|^2/\omega_s$, $\bar{\mathscr{H}}$ is given by $\bar{\mathscr{H}} = \mathscr{H}_0 + \mathscr{H}'$ with $\mathscr{H}'$ defined as

$$\mathscr{H}' = -\sum_{n\neq 0} \frac{1}{2n\omega_s}[\mathscr{H}_n, \mathscr{H}_{-n}]. \quad [6]$$

Both $\mathscr{H}_0$ and $\mathscr{H}'$ can be easily derived from Eqs. [4] and [5] as

$$\mathscr{H}_0 = \sum_{n'=-2}^{2} d^{(2)}_{n'0}(\beta_p) d^{(2)}_{0n'}(\beta_s) e^{-in'(\gamma+\omega_p t)} S_0$$

$$= 2S_0 \sum_{n'=0}^{2} d^{(2)}_{n'0}(\beta_p) d^{(2)}_{0n'}(\beta_s) \cos[n'(\gamma + \omega_p t)] \quad [7]$$

and

$$\mathscr{H}' = \sum_{n'=-4}^{4} \mathscr{H}'_{n'} e^{-in'(\gamma+\omega_p t)}$$

$$= 2 \sum_{n'=0,2,4} \mathscr{H}'_{n'} \cos[n'(\gamma + \omega_p t)]$$

$$- 2i \sum_{n'=1,3} \mathscr{H}'_{n'} \sin[n'(\gamma + \omega_p t)], \quad [8]$$

where

$$\mathscr{H}'_{n'} = \sum_{j=0,2,4} a^j(\beta_p) d^{(j)}_{0n'}(\beta_s) \sum_{n\neq 0} \frac{1}{2n\omega_s}$$

$$\times c(22j; n, -n)[S_n, S_{-n}]. \quad [9]$$

Here $a^j(\beta_p)$ is a coefficient that depends on j only, and $c(22j; n, -n)$ is the Clebsch–Gordan coefficient.

It is important to realize that $\mathscr{H}_0$ in Eq. [7] is inhomogeneous; i.e., $[\mathscr{H}_0(t_1), \mathscr{H}_0(t_2)] = 0$ for any two arbitrary times t_1 and t_2. The corresponding time-evolution operator U^0 can therefore be easily obtained by performing the integration

$$U^0(t) = \exp\left\{-i\int_0^t dt' \mathscr{H}_0(t')\right\} = U^1 U^2. \quad [10]$$

U^1 and U^2 arise from the contributions of $n' = 1$ and $n' = 2$ terms in Eq. [7], respectively, and are given by

$$U^1 = \exp\left\{-i2d^{(2)}_{1,0}(\beta_p) d^{(2)}_{0,1}(\beta_s) \frac{1}{\omega_p}\right.$$

$$\left.[\sin(\gamma + \omega_p t) - \sin(\gamma)]S_0\right\}, \quad [11]$$

and

$$U^2 = \exp\left\{-i2d^{(2)}_{2,0}(\beta_p) d^{(2)}_{0,2}(\beta_s) \frac{1}{\omega_p}\right.$$

$$\left.[\sin(2(\gamma + \omega_p t)) - \sin(2\gamma)]S_0\right\}. \quad [12]$$

The $n' = 0$ term in Eq. [7] does not contribute because $d^{(2)}_{0,0}(\beta_p)$ vanishes at $\beta_p = 54.74°$. For the centerband with respect to the spinning motion, the total evolution operator U is governed only by the Hamiltonian $\bar{\mathscr{H}}$ and can be written as $U = U^1 U^2 U^{int}$, where U^{int} is determined by the Hamiltonian $\mathscr{H}^{int} = U^{0\dagger} \mathscr{H}' U^0$

The free-induction-decay (FID) signal F originating from $\xi(t)$ can be generally represented as

$$F = \mathrm{Tr}(I_+ \xi) = \mathrm{Tr}(U^{2\dagger} U^{1\dagger} I_+ U^1 U^2 U^{int} I_x U^{int\dagger}). \quad [13]$$

Since U^1 and U^2 are both inhomogeneous, they introduce only periodic evolutions but no signal decay. The spectral linewidth is completely determined by the homogeneous Hamiltonian $\mathscr{H}^{int}$, which is of the order of $\|\mathscr{H}_D\|^2/\omega_s$. However, because $\mathscr{H}^{int}$ is a many-body Hamiltonian, it is still impossible to calculate either the details of the FID signals or the details of $\mathscr{H}^{int}$ itself. Yet, some properties can be understood without completely solving the many-body problems.

By applying the Fourier–Bessel expansion, $\exp(iz \sin \phi) = \sum_{n=-\infty}^{\infty} J_m(z) e^{in\phi}$, where J_m is the Bessel function, to the evolution operators U^1 and U^2 in Eqs. [11] and [12], it is easy to see from Eq. [8] that $\mathscr{H}^{int}$ can always be expanded to

$$\mathscr{H}^{int} = \sum_{k=-\infty}^{\infty} \mathscr{H}^{int}_k(\gamma) e^{-ik(\gamma+\omega_p t)}, \quad [14]$$

in which $\mathscr{H}^{int}_k$ is time-independent and is of the order of $\|\mathscr{H}_D\|^2/\omega_s$. Assume now that $\omega_p > \|\mathscr{H}_D\|^2/\omega_s$; then the density operator $\rho^{int} = U^{int} I_x U^{int\dagger}$ can again be solved by using the averaging method. It consists of a slowly varying term $\xi^{int}(\gamma, t)$ and the harmonic terms $\rho^{int}_k(\gamma, t)e^{-ik\omega_p}$ similar to Eq. [3]. However, unlike $\xi(t)$ in Eq. [3], ξ^{int} does not contain any modulation frequency and is governed by $d\xi^{int}/dt = -i[\overline{\mathscr{H}^{int}}, \xi^{int}]$, where the time-independent Hamiltonian $\overline{\mathscr{H}^{int}}$ is given by

$$\overline{\mathscr{H}^{int}} = \mathscr{H}^{int}_0 - \sum_{n\neq 0} \frac{1}{2n\omega_p}[\mathscr{H}^{int}_n, \mathscr{H}^{int}_{-n}]. \quad [15]$$

The harmonic terms ρ^{int}_k are, according to the averaging method, determined by $\rho^{int}_k = \omega_p^{-1}[\mathscr{H}^{int}_k e^{-ik\gamma}, \xi^{int}]$ in the first-order approximation. If $\omega_p \gg \|\mathscr{H}_D\|^2/\omega_s$ is satisfied, i.e., the peaks are well separated from each other, $\mathscr{H}^{int}_0$ dominates

the spectral linewidth, which is then proportional to $1/\omega_s$ but independent of ω_p. In addition, the effects of the harmonic terms ρ_k^{int} can be neglected in the calculations of the FID because $\|\rho_k^{int}\| \ll \|\xi^{int}\|$. The sideband patterns with respect to the precession motion are thus determined by U^1U^2 and therefore behave like those of an inhomogeneous spin system (7). At lower precession frequencies, however, $\rho_k^{int}(\gamma, t)e^{-ik\omega_p}$ contribute to the sideband patterns, and the linewidth will depend on the precession frequencies as well.

Figure 3 shows a plot of the spectral linewidth at half-height, $\Delta f_{1/2}$, versus $1/\omega_s$, recorded in two double rotors with different ratios ω_s/ω_p (5) and with precession frequencies that exceeded the linewidths. As expected, the spectral linewidth is indeed inversely proportional to ω_s. The two lines have exactly the same slope but different intercepts owing to the different shimming values of the external magnetic field. The inset to Fig. 3 is a plot of the spectral linewidth versus $1/\omega_p$ for the same value of ω_s and, as predicted above, the linewidth is independent of the precession frequency ω_p.

Another feature that can be understood without solving the complete many-body problem is the change in the sideband patterns when γ is varied from 0° to 180°. Consider the γ dependence of the operator $U^{1\dagger}Ae^{-in'\omega_p t}U^1$, where A is a γ-independent operator. Applying the Fourier–Bessel expansion for U^1, the operator $U^{1\dagger}Ae^{-in'\omega_p t}U^1$ can be expressed as

$$U^{1\dagger}Ae^{-in'\omega_p t}U^1 = \sum_{m,m'=-\infty}^{\infty} J_m(\pm z)AJ_{m'}(\mp z)e^{i(m+m'-n')\omega_p t}, \quad [16]$$

where $z = d^{(2)}_{1,0}(\beta_p)d^{(2)}_{0,1}(\beta_p)\omega_p^{-1}S_0$. $J_m(z)AJ_{m'}(-z)$ and $J_m(-z)AJ_{m'}(z)$ correspond to the cases of $\gamma = 0°$ and $\gamma = 180°$, respectively. Since $J_m(-z) = (-1)^m J_m(z)$, it can be derived easily that $J_m(z)AJ_{m'}(-z) = J_m(-z)AJ_{m'}(z)$ if $m + m'$ is even, and $J_m(z)AJ_{m'}(-z) = -J_m(-z)AJ_{m'}(z)$ if $m + m'$ is odd. In other words, changing γ from 0° to 180° leaves those terms in Eq. [16] with even $m + m'$ unchanged, but those terms with odd $m + m'$ change signs. Applying this analysis to $U^{1\dagger}\mathscr{H}'U^1$, we see from Eq. [8] that those terms with even $k = m + m' - n'$ will not be changed when γ switches from 0° to 180°, because if $m + m'$ and n' are both even then neither $J_m(z)\mathscr{H}'_{n'}J'_m(-z)$ nor $\cos[n'(\gamma + \omega_p t)]$ will change sign. Conversely, if $m + m'$ and n' are both odd, then $J_m(z)\mathscr{H}'_{n'}J'_m(-z)$ and $\sin[n'(\gamma + \omega_p t)]$ will each change sign. For similar reasons, those terms with odd $k = m + m' - n'$ will change sign. Since γ appears in U^2 only in the form $e^{i2m\gamma}$, which contains only even harmonic terms, the above conclusions hold also for $U^{2\dagger}U^{1\dagger}\mathscr{H}'U^1U^2$. This implies that $\mathscr{H}_k^{int}$ change sign if k is an odd number and remains the same if k is an even number when $\gamma = 0° \leftrightarrow 180°$. From this conclusion, we know that $\mathscr{H}^{int}$ and therefore also ξ^{int} and ρ_k^{int} with even k remain unchanged whereas ρ_k^{int} with odd k change signs when $\gamma = 0° \leftrightarrow 180°$. Similar

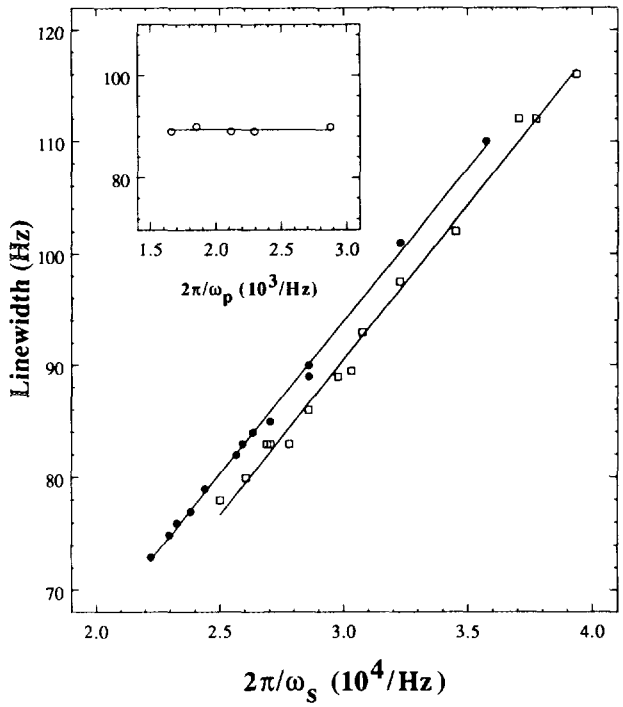

FIG. 3. The linewidth at half-height, $\Delta f_{1/2}$, plotted against the spinning frequency $(2\pi/\omega_s) \times 10^4$ using two different DOR probes. Various bearing and drive pressures are used for the inner rotors in order to produce different spinning frequencies ω_s for the same precession frequency ω_p. The overall shift between the data sets (● and □) recorded with the two different probes is due to the different shimming values of the external magnetic field. The inset shows the linewidth versus $(2\pi/\omega_p) \times 10^3$ at $\omega_s/2\pi = 3.5$ kHz.

conclusions can be drawn for $U^{2\dagger}U^{1\dagger}I_+U^1U^2$. Thus it is not difficult to see that the odd-numbered harmonic terms of the operator $U^{2\dagger}U^{1\dagger}I_+U^1U^2U^{int}I_xU^{int\dagger}$ in Eq. [13] also change signs while the even-numbered harmonic terms remain the same when $\gamma = 0° \leftrightarrow 180°$.

This effect is demonstrated experimentally by synchronizing the RF pulses with the mechanical motions of the double rotor. Figure 4 shows the DOR spectra taken at $\omega_p/2\pi = 606$ Hz with random γ, $\gamma = 0°$ and $\gamma = 180°$. Contributions from ρ_k^{int} are very small in this situation. The phases of the odd-numbered sidebands are indeed reversed while those of the even-numbered sidebands remain unchanged. When the precession frequency ω_p is reduced such that the sidebands and the centerband are strongly overlapped with each other (as in Fig. 5a, which is the same spectrum as Fig. 2b), the sideband patterns are also determined by the homogeneous interactions $\mathscr{H}^{int}$ because $\|\xi^{int}\|$ and $\|\rho_k^{int}\|$ are now comparable. Still, if we carry out the phase-reversal operation in these circumstances of strongly overlapping lines, the same phenomenon is observed as illustrated in Fig. 5b, where the spectrum is accumulated with γ alternating between 0° and 180°. The odd-numbered sidebands completely disappear owing to the phase-reversal effects. The linewidth, about 210 Hz, is much larger than that in Fig. 2c, which was measured at the same spinning fre-

quency of 2.6 kHz but at the higher precession frequency of 323 Hz. This observation confirms that $\|\xi^{int}\|$ and $\|\rho_k^{int}\|$ are comparable in Fig. 5.

CONCLUSIONS

In summary, we have demonstrated both theoretically and experimentally that the DOR technique can also serve as an effective tool for reducing the line broadening of homonuclear dipole–dipole interactions. The only requirement is that the spinning frequency ω_s be larger than the dipole–dipole interactions $\mathscr{H}_D$. The precession frequency ω_p, by contrast, can be significantly smaller than $\mathscr{H}_D$. Moreover, the homogeneous system behaves inhomogeneously with respect to the precession motion. The phase-reversal phenomenon of the odd-numbered harmonics of the NMR signals upon alternations of the phase γ may be understood without solving the details of the many-body problem.

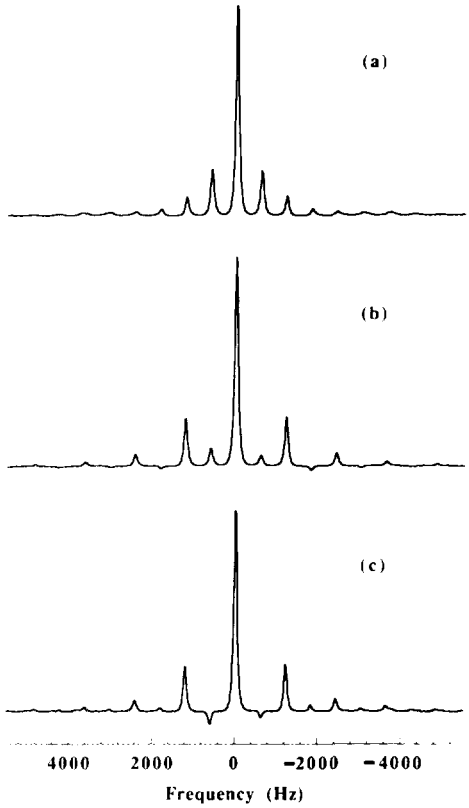

FIG. 4. ^{23}Na DOR spectra of NaCl observed for $\omega_p/2\pi$ = 606 Hz and $\omega_s/2\pi$ = 3.7 kHz. (a) DOR spectrum averaged over 300 scans with γ being random. (b) Synchronized DOR spectrum at γ = 0°. (c) Synchronized DOR spectrum at γ = 180°.

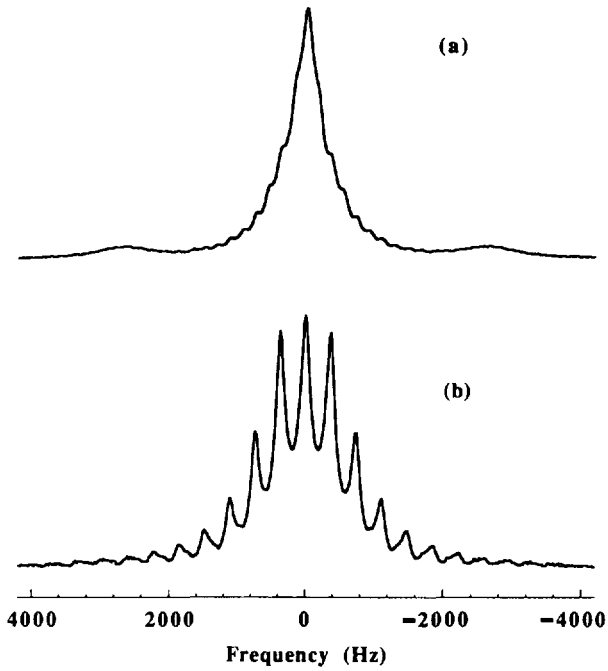

FIG. 5. ^{23}Na DOR spectra of NaCl recorded with $\omega_p/2\pi$ = 190 Hz and $\omega_s/2\pi$ = 2.6 kHz. (a) DOR spectrum averaged over 700 scans with γ being random. (b) Synchronized DOR spectrum accumulated over 128 scans with γ alternating between 0° and 180°.

ACKNOWLEDGMENTS

This work was supported by the Director, Office of Basic Energy Sciences, Materials Sciences Division, of the U.S. Department of Energy under Contract DE-AC03-76SF00098.

REFERENCES

1. E. R. Andrew, A. Bradbury, and R. G. Eades, *Arch. Sci.* **11**, 223 (1958); I. J. Lowe, *Phys. Rev. Lett.* **2**, 285 (1959).
2. A. Samoson, E. Lippmaa, and A. Pines, *Mol. Phys.* **65**, 1013 (1988).
3. A. Samoson and E. Lippmaa, *J. Magn. Reson.* **84**, 410 (1989).
4. W.-K. Rhim, A. Pines, and J. S. Waugh, *Phys. Rev. Lett.* **25**, 218 (1970).
5. Y. Wu, B. Q. Sun, A. Pines, A. Samoson, and E. Lippmaa, *J. Magn. Reson.* **89**, 297 (1990).
6. U. Haeberlen, "High Resolution NMR in Solids," Academic Press, New York, 1976; M. Mehring, "High Resolution NMR Spectroscopy in Solid, NMR," Springer, Berlin/Heidelberg, 1976.
7. M. M. Maricq and J. S. Waugh, *J. Chem. Phys.* **70**, 3300 (1979).
8. M. G. Munowitz and R. G. Griffin, *J. Chem. Phys.* **76**, 2848 (1982).
9. G. S. Harbison and H. W. Spiess, *Chem. Phys. Lett.* **124**, 128 (1986).
10. N. N. Bogolyubov and Yu. A. Mitropol'skii, "Asimptoticheskie metody v teorii nelineinykh kolebanii," Nauka, Moscow, 1974; L. L. Buishvili and M. G. Menabde, *Sov. Phys. JETP* **50**, 1176 (1979).